Astigmatic Gaussian Beam Scattering by a PEC Wedge

Ram Tuvi and Timor Melamed, *Senior Member, IEEE*

***Abstract*— We are concerned with the scattering of a 3-D time harmonic astigmatic Gaussian beam from a perfectly electric conducting wedge. The incident wave object serves as the wave propagator of the phase-space beam summation method, which is a general framework for analyzing propagation of scalar and electromagnetic fields from extended sources. We perform asymptotic analysis for the total field including fields in the transition regions identifying the corresponding wave phenomena such as reflected beams and diffraction beams.**

***Index Terms*— Asymptotic analysis, Gaussian beams (GBs), wedge diffraction.**

I. Introduction

Beam methods has been intensively investigated in the past few decades due to the advantages arising from the mutual spatial-directional locality of the beam wave objects. These wave objects serve as a basis for decomposing scalar and EM fields into a set of Gaussian beams propagators (GBPs) that are emanating over a discrete (phase-space) grid of locations and directions [1]–[3]. By applying locality considerations for some generic scattering problem, the scattered field due to each GBP can be obtained for a wide class of canonical problems [4]–[17]. By using such a library of canonical solutions, the scattering of a generic EM field from a complex scatterer can be obtained asymptotically by summing over each local interaction. Such a canonical problem is the scattering from a PEC wedge that is investigated here and presented in Fig. 1.

The diffraction of plane waves (PWs) by wedges has been explored in the literature [18], [19]. Uniform asymptotic solutions were derived in [20] and [21], where the dyadic diffraction coefficients were obtained in the form of Fresnel integrals (for a review of several asymptotic techniques in connection with electromagnetic wave scattering from wedges please refer to [22]).

Beam summation representation of the edge field of a half-plane due to a PW was obtained in [23]. In [24] and [25] a 2-D Gaussian beam (GB) scattering and a 3-D GB scattering were investigated, respectively. In this method, the diffraction field is represented by a sum of GBs, which propagate in all directions. Other publications involving beam methods and wedge scattering can be found in [26]–[28].

Manuscript received April 13, 2018; revised June 8, 2019; accepted June 15, 2019. Date of publication July 9, 2019; date of current version October 29, 2019. *(Corresponding author: Timor Melamed.)*

The authors are with the School of Electrical and Computer Engineering, Ben-Gurion University of the Negev, Beer Sheva 8410501, Israel (e-mail: timormel@bgu.ac.il).

Color versions of one or more of the figures in this article are available online at http://ieeexplore.ieee.org.

Digital Object Identifier 10.1109/TAP.2019.2925928

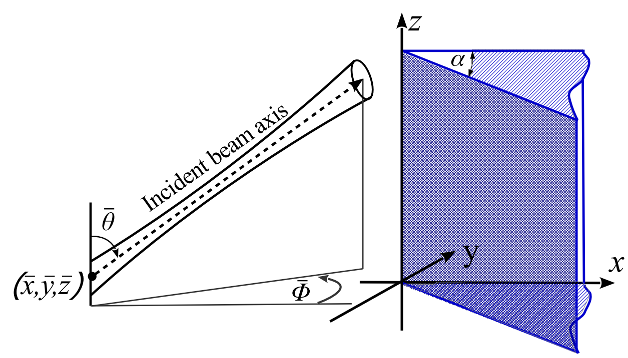

Fig. 1. Physical configuration. A GBP is impinging on a PEC wedge. The GBP is emanating from the point $(y, z) = (\bar y, \bar z)$ over the plane $x = \bar x$. The scattering object is a PEC wedge with a head angle of α.

II. Problem Definition

We briefly review here the main results of the EM frame-based beam decomposition, which was introduced in [2]. The frame-based beam summation for propagating an EM field from the $x = \bar x$ aperture is constructed on a discrete frame spatial–spectral lattice $(\bar y, \bar z, \bar\kappa_y, \bar\kappa_z)$. The lattice unit-cell dimensions satisfy

$$\Delta\bar y\Delta\bar\kappa_y = 2\pi\nu/k, \quad \Delta\bar z\Delta\bar\kappa_z = 2\pi\nu/k \tag{1}$$

where $0 \le \nu \le 1$ is the overcompleteness (or oversampling) parameter. The lattice is overcomplete for $\nu < 1$, critically complete in the Gabor limit $\nu \uparrow 1$, and for $\nu \downarrow 0$, the discrete parametrization attains the continuity limit.

The EM aperture field $\mathbf{E}_0(y, z)$ over the plane $x = \bar x$ is propagated into $x > \bar x$ via a summation over GBPs. These GBPs are emanating from the frame lattice set of points over the aperture plane $(\bar y, \bar z)$ and in the discrete set of directions that is determined by the spectral tilts $(\bar\kappa_y, \bar\kappa_z)$. The expansion coefficients a_y and a_z for each point over the frame lattice are obtained by the inner product of the aperture field with the so-called dual frame, via

$$a_y\hat{\mathbf{y}} + a_z\hat{\mathbf{z}} = \int dydz\ \mathbf{E}_0(y,z)\varphi^*(y-\bar y, z-\bar z) \times \exp[-jk(\bar\kappa_y(y-\bar y) + \bar\kappa_z(z-\bar z))] \tag{2}$$

where under the framework of Gaussian window frames

$$\varphi(y,z) = (-\nu^2 k \mathrm{Im}\Gamma/\pi)\exp[-jk\Gamma(y^2+z^2)/2]. \tag{3}$$

Here, Γ is a complex *frequency-independent* parameter with $\mathrm{Im}\Gamma < 0$, $k = \omega/c$ is the free-space wavenumber, and ν is the oversampling parameter in (1). The considerations for adjusting the expansion parameters were discussed in [17].

In the present investigation, the incident EM field is the GBP that is used in the GB summation method (see Fig. 1). Thus, the incident EM GBP that emanates from the point $(y, z) = (\bar{y}, \bar{z})$ over the $x = \bar{x}$ aperture plane is given by the PW spectral integral over the normalized wavenumbers κ_y and κ_z in the form [3]

$$\mathbf{E}^i(\mathbf{r}) = \left(\frac{k}{2\pi}\right)^2 \int d^2\kappa_s \tilde{\mathbf{E}}_0(\boldsymbol{\kappa}_s)\tilde{w}(\boldsymbol{\kappa}_s)\exp(-jk\hat{\boldsymbol{\kappa}}\cdot\mathbf{r})$$
$$\mathbf{H}^i(\mathbf{r}) = \left(\frac{k}{2\pi}\right)^2 \int d^2\kappa_s \tilde{\mathbf{H}}_0(\boldsymbol{\kappa}_s)\tilde{w}(\boldsymbol{\kappa}_s)\exp(-jk\hat{\boldsymbol{\kappa}}\cdot\mathbf{r}) \quad (4)$$

where $\mathbf{r} = (x, y, z)$ is the observation vector in the conventional cartesian coordinate system and $\hat{\boldsymbol{\kappa}}$ is the unit vector

$$\hat{\boldsymbol{\kappa}} = (\kappa_x, \boldsymbol{\kappa}_s), \quad \boldsymbol{\kappa}_s = (\kappa_y, \kappa_z) \quad (5)$$

with

$$\kappa_x = \sqrt{1-\kappa_y^2-\kappa_z^2}, \quad \mathrm{Re}\kappa_x \geq 0,\ \mathrm{Im}\kappa_x \leq 0 \quad (6)$$

denoting the longitudinal (normalized) wavenumber. In (4), the spectral distributions $\tilde{\mathbf{E}}_0$ and $\tilde{\mathbf{H}}_0$ are given by

$$\tilde{\mathbf{E}}_0(\boldsymbol{\kappa}_s) = a_y\left(\hat{\mathbf{y}} - \frac{\kappa_y}{\kappa_x}\hat{\mathbf{x}}\right) + a_z\left(\hat{\mathbf{z}} - \frac{\kappa_z}{\kappa_x}\hat{\mathbf{x}}\right)$$
$$\tilde{\mathbf{H}}_0(\boldsymbol{\kappa}_s) = \eta_0^{-1}\hat{\boldsymbol{\kappa}} \times \tilde{\mathbf{E}}_0(\boldsymbol{\kappa}_s) \quad (7)$$

where

$$\tilde{w}(\boldsymbol{\kappa}_s) = \frac{2\pi}{jk\Gamma}\exp(jk\hat{\boldsymbol{\kappa}}\cdot\bar{\mathbf{r}})\exp[jk\tilde{\Omega}_b(\boldsymbol{\kappa}_s)]$$
$$\tilde{\Omega}_b(\boldsymbol{\kappa}_s) = \frac{(\kappa_y-\bar{\kappa}_y)^2+(\kappa_z-\bar{\kappa}_z)^2}{2\Gamma}. \quad (8)$$

Here, $\bar{\mathbf{r}} = (\bar{x}, \bar{y}, \bar{z})$. In (7), a_y and a_z are the expansion coefficients in (2). In (4)–(8), we denote PW spectral constituents by an over tilde ($\sim$). In the following equations, we suppress the $(\boldsymbol{\kappa}_s)$ explicit dependence (i.e., all tilded quantities are functions of $\boldsymbol{\kappa}_s$).

The beam propagator in (4) emanates from the point $\bar{\mathbf{r}}$ and propagates in the direction of the unit vector

$$\hat{\bar{\kappa}} = (\bar{\kappa}_x, \bar{\kappa}_y, \bar{\kappa}_z) = (\sin\bar{\theta}\cos\bar{\phi}, \sin\bar{\theta}\sin\bar{\phi}, \cos\bar{\theta}) \quad (9)$$

where $\bar{\kappa}_x = (1-\bar{\kappa}_y^2-\bar{\kappa}_z^2)^{1/2}$ with $\mathrm{Re}\bar{\kappa}_x \geq 0$. We restrict the current investigation to propagating GBPs for which we assume that $\bar{\kappa}_y^2+\bar{\kappa}_z^2 \leq 1-\Delta_{\kappa_s}$, where Δ_{κ_s} denotes the spectral width of $\tilde{w}(\boldsymbol{\kappa}_s)$.

We consider the scattering of the EM GBP in (4) from a PEC wedge (see Fig. 1). The medium is vacuum with ε_0, μ_0 denoting the free space permittivity and permeability, respectively. The wedge is infinite in the z direction, with a head angle of $\alpha < \pi$.

III. Asymptotic Analysis

The incident GBP is defined by the spectral integral in (4). In this section, we evaluate the asymptotic total fields by replacing each PW in (4) with the well-known PW scattered field and evaluate asymptotically the resulting integrals.

A. Spectral Integrals

The solution of PW scattering by a wedge was derived in [20] and [21]. The procedure applies the two Hertz potentials that are corresponding to either the electric (TM) or the magnetic (TE) z-components of the incident PW. The EM fields are derived from the potentials by applying the standard differential operators in [21].

We define the incident electric and magnetic *potentials*, $\Psi^i_{A,F}$, that are corresponding to either the electric (TM) or the magnetic (TE) z-components of the incident fields in (4), respectively, i.e.,

$$\Psi^i_{A,F}(\mathbf{r}) = \left(\frac{k}{2\pi}\right)^2 \int d^2\kappa_s \tilde{\Psi}_{A_0,F_0}\tilde{w}(\boldsymbol{\kappa}_s)\exp(-jk\hat{\boldsymbol{\kappa}}\cdot\mathbf{r}). \quad (10)$$

Here,

$$\tilde{\Psi}_{A_0} = \frac{j\omega\varepsilon_0}{(k_t)^2}\tilde{E}_{0z}, \quad \tilde{\Psi}_{F_0} = \frac{j\omega\mu_0}{(k_t)^2}\tilde{H}_{0z} \quad (11)$$

where

$$k_t = k\kappa_t,\ \kappa_t = \sqrt{\kappa_x^2+\kappa_y^2}, \quad \mathrm{Re}(\kappa_t) > 0 \quad (12)$$

and $\tilde{E}_{0z}$ and $\tilde{H}_{0z}$ are defined in (7).

Next, in order to evaluate the *total field potentials*, we replace the PWs in (10) with its wedge response [20], [21]. Thus, the total potentials are given by

$$\Psi_{A,F}(\mathbf{r}) = \left(\frac{k}{2\pi}\right)^2 \int d^2\kappa_s \tilde{\Psi}_{A_0,F_0}\tilde{w}\exp(-jk\kappa_z z)\tilde{g}_{s,h}(\rho,\phi) \quad (13)$$

where $\tilde{w}$ is given in (8) and $\tilde{g}_{s,h}(\rho,\phi)$ denotes the soft (TM) and hard (TE) PW response of a wedge to a 2-D incident PW $\exp[-jk_t\rho\cos(\phi-\tilde{\phi}_0)]$ (see also [29]). Here and henceforth, (ρ, ϕ, z) denotes the cylindrical coordinates.

The representation of the total potentials in (13) is an exact representation. For the TM polarization, the EM fields are derived from the electric potential by applying the differential operators [21]

$$E_\rho = (j\omega\varepsilon_0)^{-1}\partial_\rho\partial_z\Psi_A, \quad H_\rho = \rho^{-1}\partial_\phi\Psi_A$$
$$E_\phi = (j\omega\varepsilon_0\rho)^{-1}\partial_\phi\partial_z\Psi_A, \quad H_\phi = -\partial_\rho\Psi_A$$
$$E_z = (j\omega\varepsilon_0)^{-1}\left(\partial_z^2+k^2\right)\Psi_A, \quad H_z = 0. \quad (14)$$

The TE fields are obtained from Ψ_F via

$$E_\rho = -\rho^{-1}\partial_\phi\Psi_F, \quad H_\rho = (j\omega\mu_0)^{-1}\partial_\rho\partial_z\Psi_F$$
$$E_\phi = \partial_\rho\Psi_F, \quad H_\phi = (j\omega\mu_0\rho)^{-1}\partial_\phi\partial_z\Psi_F$$
$$E_z = 0, \quad H_z = (j\omega\mu_0)^{-1}\left(\partial_z^2+k^2\right)\Psi_F. \quad (15)$$

For large values of $k_t\rho$, one may replace the integral forms of $\tilde{g}_{s,h}(\rho,\phi)$ with their asymptotic forms [20]

$$\tilde{g}_{s,h}(\rho,\phi) = \tilde{g}(\rho,\Phi^-) + \tau\tilde{g}(\rho,\Phi^+)$$
$$\tilde{g}(\rho,\phi) \sim \tilde{g}^{\mathrm{GO}}(\rho,\phi) + \tilde{g}^d(\rho,\phi) \quad (16)$$

where $\tilde{g}^{\mathrm{GO}}$ and $\tilde{g}^d$ are termed the geometrical optics (GOs) and the diffraction Green's functions (GFs) and

$$\tau = \begin{cases} -1, & \text{TM (soft) case} \\ 1, & \text{TE (hard) case.} \end{cases} \quad (17)$$

is used to tag the TE/TM potentials.

The GO term is given by

$$\tilde{g}^{\mathrm{GO}}(\rho,\phi) = \sum_m U(\pi - |-\tilde{\Phi}^{\mp} + 2m\pi N|) \times \exp[jk_t\rho\cos(2mN\pi - \Phi^{\mp})] \quad (18)$$

where $U(t)$ denotes the (Heaviside) unit step function

$$\tilde{\Phi}^{\mp} = \phi \mp \tilde{\phi}_0, \quad N = (2\pi - \alpha)/\pi \quad (19)$$

and $\tilde{\phi}_0$ is related to the spectral variables in (5) via

$$\hat{\boldsymbol{\kappa}} = (-\cos\tilde{\phi}_0\sin\tilde{\theta}_0, -\sin\tilde{\phi}_0\sin\tilde{\theta}_0, \cos\tilde{\theta}_0). \quad (20)$$

In (16), $\tilde{g}^d_{s,h}$ denote the (soft/hard) diffraction GFs

$$\tilde{g}^d_{s,h}(\rho,\phi) \sim \frac{\exp(-jk_t\rho)}{\sqrt{\rho}}\tilde{D}_{s,h}(\phi,\phi_0) \quad (21)$$

where $\tilde{D}_{s,h}$ denote the uniform diffraction coefficients

$$\begin{aligned}\tilde{D}_{s,h}(\phi) = (\sin\tilde{\theta}_0)^{-1}\{&d^+(\tilde{\Phi}^-)F[k_t\rho\sin\tilde{\theta}_0 a^+(\tilde{\Phi}^-)]\\ &+d^-(\tilde{\Phi}^-)F[k_t\rho\sin\tilde{\theta}_0 a^-(\tilde{\Phi}^-)]\\ &+\tau d^+(\tilde{\Phi}^+)F[k_t\rho\sin\tilde{\theta}_0 a^+(\tilde{\Phi}^+)]\\ &+\tau d^-(\tilde{\Phi}^+)F[k_t\rho\sin\tilde{\theta}_0 a^-(\tilde{\Phi}^+)]\}\end{aligned} \quad (22)$$

where $\tilde{\phi}_0$ and $\tilde{\theta}_0$ given in (20), and $\tilde{\Phi}^{\mp}$ and τ are given in (19) and (17), respectively. In (22)

$$F(x) = 2j|\sqrt{x}|\exp(jx)\int_{|\sqrt{x}|}^{\infty}\exp(-j\xi^2)d\xi \quad (23)$$

denotes the (Fresnel) transition function, and

$$\begin{aligned}d^{\pm}(\Phi) &= -\frac{1}{2N}\frac{\exp(-j\pi/4)}{\sqrt{2\pi k}}\cot\left(\frac{\pi \pm \Phi}{2N}\right)\\ a^{\pm}(\Phi) &= 2\cos^2\left(\frac{2N\pi n^{\pm}(\Phi) - \Phi}{2}\right)\end{aligned} \quad (24)$$

with $n^{\pm}$ is an integer which mostly satisfies the condition

$$n^{\pm}(\Phi) = (\mp\pi + \Phi)/(2\pi N). \quad (25)$$

The high-frequency spectral representations of the total potentials is obtained by inserting (16) into (13). The resulting potentials consist of a GOs potential, $\Psi^{\mathrm{GO}}_{A,F}$, and a diffraction term, $\Psi^d_{A,F}$, i.e.,

$$\Psi_{A,F}(\mathbf{r}) \sim \Psi^{\mathrm{GO}}_{A,F}(\mathbf{r}) + \Psi^d_{A,F}(\mathbf{r}). \quad (26)$$

The GO term reads

$$\Psi^{\mathrm{GO}}_{A,F}(\mathbf{r}) = \Psi^i_{A,F}(\mathbf{r}) + \tau\Psi^{r1}_{A,F}(\mathbf{r}) + \tau\Psi^{r2}_{A,F}(\mathbf{r}). \quad (27)$$

The GO term consists of three wave fields: the incident potential, $\psi^i_{A,F}$, and reflected potentials from $\phi = 0$ and the from the $\phi = N\pi$ surfaces that are denoted by $\psi^{r1}_{A,F}$ and $\psi^{r2}_{A,F}$, respectively. These terms are given by

$$\begin{aligned}\Psi^i_{A,F}(\mathbf{r}) &= \int d^2\kappa_s\tilde{\Psi}_{A_0,F_0}\frac{k}{2\pi j\Gamma}\exp\left(-jk\tilde{\Omega}^{\mathrm{GO}}_i\right) \times U(\pi - |\phi - \tilde{\phi}_0|)\\ \Psi^{r1}_{A,F}(\mathbf{r}) &= \int d^2\kappa_s\tilde{\Psi}_{A_0,F_0}\frac{k}{2\pi j\Gamma}\exp\left(-jk\tilde{\Omega}^{\mathrm{GO}}_{r1}\right) \times U(\pi - |\phi + \tilde{\phi}_0|)\end{aligned} \quad (28)$$

and

$$\Psi^{r2}_{A,F}(\mathbf{r}) = \int d^2\kappa_s\tilde{\Psi}_{A_0,F_0}\frac{k}{2\pi j\Gamma}\exp\left(-jk\tilde{\Omega}^{\mathrm{GO}}_{r2}\right) \times U[\pi - |2\pi N - (\phi + \tilde{\phi}_0)|]. \quad (29)$$

Here, $\tilde{\theta}_0$ and $\tilde{\phi}_0$ are given in (20) and N is given in (19).

In (28) and (29), the phase terms are given by

$$\begin{aligned}\tilde{\Omega}^{\mathrm{GO}}_i &= \kappa_x(x - \bar{x}) + \kappa_y(y - \bar{y}) + \kappa_z(z - \bar{z}) - \tilde{\Omega}_b\\ \tilde{\Omega}^{\mathrm{GO}}_{r1} &= \kappa_x(x - \bar{x}) - \kappa_y(y + \bar{y}) + \kappa_z(z - \bar{z}) - \tilde{\Omega}_b\end{aligned} \quad (30)$$

and

$$\begin{aligned}\tilde{\Omega}^{\mathrm{GO}}_{r2} = &\kappa_x(x_{r2}\cos\alpha - y_{r2}\sin\alpha - \bar{x}) - \tilde{\Omega}_b\\ &- \kappa_y(x_{r2}\sin\alpha + y_{r2}\cos\alpha + \bar{y}) + \kappa_z(z - \bar{z})\end{aligned} \quad (31)$$

where $\tilde{\Omega}_b$ is given in (8). In (31), we use the rotated coordinates x_{r2}, y_{r2} that are defined by

$$\begin{bmatrix} x_{r2} \\ y_{r2} \end{bmatrix} = \begin{bmatrix} \cos\alpha & -\sin\alpha \\ \sin\alpha & \cos\alpha \end{bmatrix}\begin{bmatrix} x \\ y \end{bmatrix}. \quad (32)$$

The diffraction potentials in (26) are given by

$$\Psi^d_{A,F}(\mathbf{r}) = \int d^2\kappa_s\frac{k\tilde{\Psi}_{A_0,F_0}}{2\pi j\Gamma}\exp[-jk\tilde{\Omega}^d(\mathbf{r})]\tilde{D}_{s,h}(\phi)\frac{\sqrt{\kappa_t}}{\sqrt{\rho}} \quad (33)$$

where κ_t is defined after (11) and the phase

$$\tilde{\Omega}^d(\mathbf{r}) = \kappa_t\rho + \kappa_z(z - \bar{z}) - \kappa_x\bar{x} - \kappa_y\bar{y} - \tilde{\Omega}_b. \quad (34)$$

In (33), the uniform (soft or hard) diffraction coefficients $\tilde{D}_{s,h}$ are given in (22). Next we evaluate the integrals in (28), (29), and (33) asymptotically.

B. Transition Regions

The integrands in (28) and (29) contain Heaviside functions and the integrands in (33) include diffraction coefficients with exponentials terms. Each term in the PW solutions (see [21]) is discontinuous over the *spectral transition regions* that are obtained by setting the Heaviside arguments in (28) and (29) to zero, giving

$$|\phi \mp \tilde{\phi}_0| = \pi, \quad |2\pi N - (\phi + \tilde{\phi}_0)| = \pi. \quad (35)$$

The $\mp$ in the first term in (35) corresponds to the incident or reflected from $\phi = 0$ potentials, and the second term is the spectral transition region of the reflected potential from the $\phi = N\pi$ surface. Over these spectral regions, the integrands in (28), (29), and (33) are discontinuous.

Next, we define the *beam transition regions* using the angle

$$\bar{\phi}_0 = \bar{\phi} + \pi(2m - 1) \quad (36)$$

where $\bar{\phi}$ is given in (9) and m being the integer that sets $0 \le \bar{\phi}_0 \le 2\pi$. By setting $\tilde{\phi}_0 = \bar{\phi}_0$ in (35), we obtain

$$|\phi \mp \bar{\phi}_0| = \pi, \quad |2\pi N - (\phi + \bar{\phi}_0)| = \pi. \quad (37)$$

C. Observation Points Outside the Transition Regions

Outside the transition regions, the Heaviside functions in (28) and (29) equal 1 or 0, and the Fresnel function in $\tilde{D}_{s,h}$ in (33) can be approximated by 1. This approximation is valid for observation points that satisfy $k_t\rho a^{\pm}(\tilde{\Phi}^{\pm}) > 10$. For these points, we can evaluate each of the integrals separately.

1) GO Potentials: The integrals in (28) and (29) can be evaluated asymptotically using standard beam-type asymptotics [30]. In this procedure, the real *on-axis* stationary points are evaluated in closed form. By using these points, the *off-axis* stationary points are approximated for near-axis observation points and the integral is evaluated asymptotically in closed form. The resulting asymptotic fields are in the form of paraxial GBs.

We begin by applying this procedure to the incident and the $\phi = 0$ surface-reflected beams in (28). To that end, we introduce the local beam coordinates, $\mathbf{r}_b$, via

$$\begin{bmatrix} x_b \\ y_b \\ z_b \end{bmatrix} = \begin{bmatrix} \bar{\kappa}_x\bar{\kappa}_y\bar{\kappa}_s^{-1} & \bar{\kappa}_x\bar{\kappa}_z\bar{\kappa}_s^{-1} & -\bar{\kappa}_s \\ -\bar{\kappa}_z\bar{\kappa}_s^{-1} & \bar{\kappa}_y\bar{\kappa}_s^{-1} & 0 \\ \bar{\kappa}_y & \bar{\kappa}_z & \bar{\kappa}_x \end{bmatrix} \begin{bmatrix} \pm y - \bar{y} \\ z - \bar{z} \\ x - \bar{x} \end{bmatrix} \tag{38}$$

where we define

$$\bar{\kappa}_s = \sqrt{\bar{\kappa}_y^2 + \bar{\kappa}_z^2}. \tag{39}$$

The $\pm$ signs in (38) correspond to either the incident or reflected beam, respectively. Using these local coordinates, we follow essentially the procedure in [30] and evaluate the localized integral asymptotically. The resulting GO potentials take the GB form

$$\Psi_{A,F}^{i}(\mathbf{r}) \sim U\big(\pi - |\phi - \bar{\phi}_0|\big)\bar{\Psi}_{A_0,F_0} \times \sqrt{\frac{\Gamma_x(z_b)}{\Gamma_x(0)}}\sqrt{\frac{\Gamma_y(z_b)}{\Gamma_y(0)}}\exp\big[-jk\mathbf{\Omega}^{\mathrm{GO}}(\mathbf{r}_b)\big] \tag{40}$$

$$\Psi_{A,F}^{r1}(\mathbf{r}) \sim U\big(\pi - |\phi + \bar{\phi}_0|\big)\bar{\Psi}_{A_0,F_0} \times \sqrt{\frac{\Gamma_x(z_b)}{\Gamma_x(0)}}\sqrt{\frac{\Gamma_y(z_b)}{\Gamma_y(0)}}\exp\big[-jk\mathbf{\Omega}^{\mathrm{GO}}(\mathbf{r}_b)\big] \tag{41}$$

where we define $\bar{\Psi}_{A_0,F_0} = \tilde{\Psi}_{A_0,F_0}(\bar{\kappa}_y, \bar{\kappa}_z)$. In (40) and (41), $\mathbf{r}_b$ is given in (38), and the GO phase is given by

$$\mathbf{\Omega}^{\mathrm{GO}}(\mathbf{r}_b) = z_b + \frac{1}{2}\big[x_b^2\Gamma_x(z_b) + y_b^2\Gamma_y(z_b)\big] \tag{42}$$

where

$$\Gamma_x(z_b) = \frac{1}{\Gamma^{-1}\bar{\kappa}_x^2 + z_b}, \quad \Gamma_y(z_b) = \frac{1}{\Gamma^{-1} + z_b} \tag{43}$$

are the complex curvatures of the beams.

The GBs in (40) and (41) are in the form of a standard astigmatic GBPs [3]. The beam peaks over the so-called beam-axis that is obtained by setting $x_b = y_b = 0$ in (38), given

$$\pm(y - \bar{y}) = (x - \bar{x})\bar{\kappa}_y/\bar{\kappa}_x, \quad z - \bar{z} = (x - \bar{x})\bar{\kappa}_z/\bar{\kappa}_x. \tag{44}$$

This condition implies that the reflected beam axis satisfies Snell's law with respect to $\phi = 0$ surface. Using in (43)

$$\Gamma^{-1} = -Z + jF \tag{45}$$

the e^{-1} beam widths in the x_b, y_b directions are given by

$$w_{x_b}(z_b) = \sqrt{\frac{2}{k}F\bar{\kappa}_x^2}\left[1 + \left(\frac{z_b - Z\bar{\kappa}_x^2}{F\bar{\kappa}_x^2}\right)^2\right]^{\frac{1}{2}}$$

$$w_{y_b}(z_b) = \sqrt{\frac{2}{k}F}\left[1 + \left(\frac{z_b - Z}{F}\right)^2\right]^{\frac{1}{2}}. \tag{46}$$

Thus, the beam waists are located in $x_b = Z\bar{\kappa}_x^2$ and $y_b = Z$ and the collimation lengths in x_b and y_b are $F\bar{\kappa}_x^2$ and F, respectively.

The asymptotic form of the $\phi = N\pi$ *surface* reflected beam in (29), $\psi_{A,F}^{r2}$, is obtained by using the local beam coordinates, $r_{b_{r2}} = (x_{b_{r2}}, y_{b_{r2}}, z_{b_{r2}})$ that are defined by

$$\begin{bmatrix} x_{b_{r2}} \\ y_{b_{r2}} \\ z_{b_{r2}} \end{bmatrix} = \begin{bmatrix} \bar{\kappa}_x\bar{\kappa}_y\bar{\kappa}_s^{-1} & \bar{\kappa}_x\bar{\kappa}_z\bar{\kappa}_s^{-1} & -\bar{\kappa}_s \\ -\bar{\kappa}_z\bar{\kappa}_s^{-1} & \bar{\kappa}_y\bar{\kappa}_s^{-1} & 0 \\ \bar{\kappa}_y & \bar{\kappa}_z & \bar{\kappa}_x \end{bmatrix} \times \begin{bmatrix} -(\sin\alpha x_{r2} + \cos\alpha y_{r2}) - \bar{y} \\ z - \bar{z} \\ \cos\alpha x_{r2} - \sin\alpha y_{r2} - \bar{x} \end{bmatrix} \tag{47}$$

where x_{r2}, y_{r2} are given by (32) and $\bar{\kappa}_s$ is given in (39). Using the paraxial approximation, the $\phi = N\pi$ surface potential is evaluated asymptotic by

$$\Psi_{A,F}^{r2}(\mathbf{r}) \sim U(\pi - |\phi + \bar{\phi}_0 - 2\pi N|)\bar{\Psi}_{A_0,F_0} \times \sqrt{\frac{\Gamma_x(z_{b_{r2}})}{\Gamma_x(0)}}\sqrt{\frac{\Gamma_y(z_{b_{r2}})}{\Gamma_y(0)}}\exp\big[-jk\mathbf{\Omega}^{\mathrm{GO}}(\mathbf{r}_{b_{r2}})\big]$$

$$\mathbf{\Omega}_{r2}^{\mathrm{GO}}(\mathbf{r}_{b_{r2}}) = z_{b_{r2}} + \frac{1}{2}\big[x_{b_{r2}}^2\Gamma_x(z_{b_{r2}}) + y_{b_{r2}}^2\Gamma_y(z_{b_{r2}})\big] \tag{48}$$

where

$$\Gamma_x(z_{b_{r2}}) = \frac{1}{\Gamma^{-1}\bar{\kappa}_x^2 + z_{b_{r2}}}, \quad \Gamma_y(z_{b_{r2}}) = \frac{1}{\Gamma^{-1} + z_{b_{r2}}}. \tag{49}$$

The result above is in the form of GBP. The complex curvatures of the beam are given by (49), and the beam widths in the $x_{b_{r2}}, y_{b_{r2}}$ axes are given by

$$w_{x_{b_{r2}}}(z_{b_{r2}}) = \sqrt{\frac{2}{k}F\bar{\kappa}_x^2}\left[1 + \left(\frac{z_{b_{r2}} - Z\bar{\kappa}_x^2}{F\bar{\kappa}_x^2}\right)^2\right]^{\frac{1}{2}}$$

$$w_{y_{b_{r2}}}(z_{b_{r2}}) = \sqrt{\frac{2}{k}F}\left[1 + \left(\frac{z_{b_{r2}} - Z}{F}\right)^2\right]^{\frac{1}{2}}. \tag{50}$$

The collimation lengths in $x_{b_{r2}}$ and $y_{b_{r2}}$ are $F\bar{\kappa}_x^2$ and F, respectively. Finally, we note that the beam peaks for [see (44)]

$$-(\sin\alpha x_{r2} + \cos\alpha y_{r2} + \bar{y}) = (\cos\alpha x_{r2} - \sin\alpha y_{r2} - \bar{x})\bar{\kappa}_y/\bar{\kappa}_x$$
$$z - \bar{z} = (\cos\alpha x_{r2} - \sin\alpha y_{r2} - \bar{x})\bar{\kappa}_z/\bar{\kappa}_x. \tag{51}$$

By setting $\phi_r = \bar{\phi} + \alpha$, one concludes that the reflected beam axis satisfies Snell's law with respect to the $\phi = N\pi$ surface.

2) Diffraction Potentials: The diffraction potentials in (33) can be evaluated asymptotically following the procedure in [30], resulting in:

$$\Psi_{A,F}^{d}(\mathbf{r}) \sim \frac{\Gamma^{-1}}{\sqrt{\det\mathbf{q}_2}}\bar{\Psi}_{A_0,F_0}\bar{D}_{s,h}\frac{\sqrt{\sin\bar{\theta}}}{\sqrt{\rho}} \times \exp\left[-jk\left(q_0 - \frac{1}{2}\mathbf{q}_1^t\mathbf{q}_2^{-1}\mathbf{q}_1\right)\right] \tag{52}$$

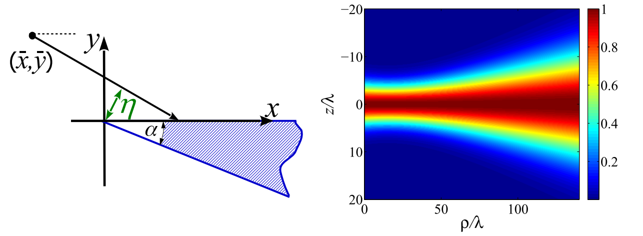

(a) (b)

Fig. 2. Diffraction potentials. (a) Diffraction stimulation parameter η in (58). (b) Cylindrical diffraction GB in (60) for $Z = 20\lambda$, $F = 50\lambda$, and $z^i_{b_0} = 5\lambda$.

where $\bar{D}_{s,h}$ are the soft/hard diffraction coefficients in (22) that are sampled at $\tilde{\phi}_0 = \bar{\phi}_0$, $\tilde{\theta} = \bar{\theta}$

$$q_0 = \sqrt{1-\bar{\kappa}_z^2}\,\rho + \bar{\kappa}_z(z-\bar{z}) - \bar{\kappa}_x\bar{x} - \bar{\kappa}_y\bar{y} \tag{53}$$

$$\mathbf{q}_1 = \begin{bmatrix} \partial_{\kappa_y}\tilde{\Omega}^d|_{\bar{\kappa}_s} \\ \partial_{\kappa_z}\tilde{\Omega}^d|_{\bar{\kappa}_s} \end{bmatrix}, \quad \partial_{\kappa_y}\tilde{\Omega}^d|_{\bar{\kappa}_s} = \frac{\bar{\kappa}_y}{\bar{\kappa}_x}\bar{x} - \bar{y}$$
$$\partial_{\kappa_z}\tilde{\Omega}^d|_{\bar{\kappa}_s} = z - \bar{z} - \rho\frac{\bar{\kappa}_z}{\sqrt{1-\bar{\kappa}_z^2}} + \frac{\bar{\kappa}_z}{\bar{\kappa}_x}\bar{x} \tag{54}$$

and $\mathbf{q}_2$ is the Hessian matrix with

$$\partial^2_{\kappa_y^2}\tilde{\Omega}^d|_{\bar{\kappa}_s} = \bar{x}\frac{\bar{\kappa}_x^2+\bar{\kappa}_y^2}{\bar{\kappa}_x^3} - \Gamma^{-1}, \quad \partial^2_{\kappa_y\kappa_z}\tilde{\Omega}^d|_{\bar{\kappa}_s} = -\bar{x}\frac{\bar{\kappa}_y\bar{\kappa}_z}{\bar{\kappa}_x^3}$$
$$\partial^2_{\kappa_z^2}\tilde{\Omega}^d|_{\bar{\kappa}_s} = -\rho\frac{1}{\left(1-\bar{\kappa}_z^2\right)^{3/2}} + \bar{x}\frac{\bar{\kappa}_x^2+\bar{\kappa}_z^2}{\bar{\kappa}_x^3} - \Gamma^{-1}. \tag{55}$$

Next we examine the diffraction field structure. First we consider the special case of a normally incident beam (the oblique incidence is discussed later). By setting $\bar{\kappa}_z = 0$ in (53)–(55), the diffraction field in (52) takes the form

$$\Psi^d_{A,F}(\mathbf{r}) \sim \frac{1}{\Gamma}\sqrt{\frac{\Gamma_{x0}\cos^2\bar{\phi}}{\rho+\Gamma_{y_0}^{-1}}}\,\bar{\Psi}_{A_0,F_0}\bar{D}_{s,h}\frac{1}{\sqrt{\rho}}$$
$$\times \exp\left(-jkz^i_{b_0}\right)\exp\left[-jk\Omega^d_s(\eta)\right]$$
$$\times \exp\left[-jk\Omega^d_b(\rho,z)\right] \tag{56}$$

where $z^i_{b_0}$ denotes the incident beam coordinate z^i_b in (38) that is sampled at the edge (i.e., at [x = 0, y = 0]), Γ_{x_0} and Γ_{y_0} are the incident beam curvatures at the edge

$$\Omega^d_s(\eta) = \frac{1}{2}\Gamma_{x0}\eta^2, \quad \Omega^d_b(\rho,z) = \rho + \frac{1}{2}\frac{(z-\bar{z})^2}{\rho+\Gamma_{y_0}^{-1}} \tag{57}$$

and

$$\eta = |\bar{y}\cos\bar{\phi} - \bar{x}\sin\bar{\phi}|. \tag{58}$$

By using (58), η is identified as the distance of the beam-axis from the edge [see Fig. 2(a)].

The phase term $kz^i_{b_0}$ in (56) is identified as the incident beam phase at the edge. The second ("stimulation") exponential term of Ω^d_s is a space-independent one for which the potential is attenuated according to

$$\exp\left(-k\eta^2\mathrm{Im}\Gamma_{x0}/2\right) = \exp\left[-\left(\eta/w^i_{x_{b0}}\right)^2\right] \tag{59}$$

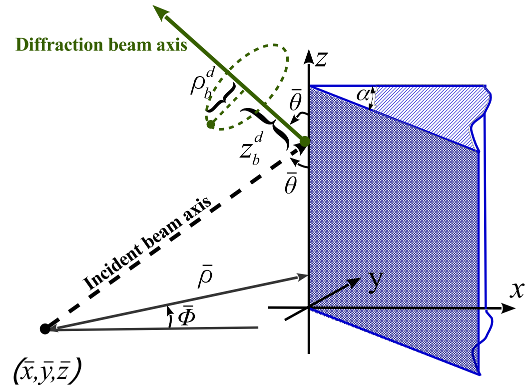

Fig. 3. Local diffraction beam coordinates. The diffraction potentials consist of the beam field in (64) in the local coordinates ρ^d_b and z^d_b in (61).

where $w^i_{x_{b0}}$ denotes the incident beamwidth, w_{x_b}, of (46) over the edge. Thus, diffraction is stimulated only when the beam displacement from the edge is on the scale of the incident beamwidth, similar to the 2-D results in [24].

The third exponential phase in (56), Ω^d_b, is of a form of a *cylindrical GB* that propagates along the ρ-axis and exhibit a Gaussian decay along the z-axis. Here, Γ_{y_0} is the diffraction beam complex curvature. The decay of the diffraction beam is given by

$$\exp\left[-\frac{k}{2}F\frac{(z-\bar{z})^2}{\left(\rho+z^i_{b_0}-Z\right)^2+F^2}\right] \tag{60}$$

where F and Z are given by (45). Thus, F is identified as the diffraction GB collimation length and $Z - z^i_{b_0}$ as its waist location [see Fig. 2(b)].

We now discuss the general case of oblique incidence for which $\bar{\kappa}_z = \cos\bar{\theta} \neq 0$. First, we note that the first term of $\mathbf{q}_1$ in (54) is independent of $\bar{\theta}$. Thus, η in (58) that parameterized the proximity of the beam axis to the edge is also valid for oblique incidence, and the diffraction beam is excited only if the incident beam passes close to the edge.

Next we examine the diffraction beam structure, assuming that the incident beam axis intersects the wedge edge, i.e., for $\eta = 0$. To that extent, we introduce the local (diffraction) beam coordinates, (ρ^d_b, z^d_b), that are defined for a given observation point (ρ, z) via

$$\begin{bmatrix}\rho^d_b \\ z^d_b\end{bmatrix} = \begin{bmatrix}\cos\bar{\theta} & -\sin\bar{\theta} \\ \sin\bar{\theta} & \cos\bar{\theta}\end{bmatrix}\begin{bmatrix}\rho \\ z-\bar{z}^i_0\end{bmatrix} \tag{61}$$

where

$$\bar{z}^i_0 = \bar{z} + \bar{\rho}\cot\bar{\theta}, \quad \bar{\rho} = \sqrt{\bar{x}^2+\bar{y}^2} \tag{62}$$

is identified as the (z-axis) point of intersection of the incident beam and the edge (see Fig. 3).

By using the beam coordinates in (61), we evaluate the Gaussian term in (52) as

$$q_0 - \frac{1}{2}\mathbf{q}_1^t\mathbf{q}_2^{-1}\mathbf{q}_1 = z^d_b + \bar{\rho}/\sin\bar{\theta} - \frac{1}{2}\frac{\left(\rho^d_b\right)^2}{\sin^2\bar{\theta}\det\mathbf{q}_2}. \tag{63}$$

Note that the determinant of $\mathbf{q}_2$ in (55) depends on ρ, i.e., on both ρ_b^d and z_b^d. In order to put the Gaussian term in a conventional form, we apply here the paraxial approximation, for which $\rho = z_b^d \sin\bar{\theta} - \rho_b^d \cos\bar{\theta} \approx z_b^d \sin\bar{\theta}$ and the Gaussian term yields

$$q_0 - \frac{1}{2}\mathbf{q}_1^t \mathbf{q}_2^{-1}\mathbf{q}_1 = \bar{\rho}/\sin\bar{\theta} + z_b^d + \frac{1}{2}\frac{\left(\rho_b^d\right)^2}{z_b^d - \bar{Z}^d} \tag{64}$$

where

$$\bar{Z}^d = \frac{\bar{\rho}}{\cos^2\bar{\phi}}\left(\bar{\kappa}_x^2 + \bar{\kappa}_y^2\right) - \frac{\bar{\rho}^2\bar{\kappa}_y^2\bar{\kappa}_z^2}{\bar{\rho}\cos^2\bar{\phi} - \Gamma^{-1}\bar{\kappa}_x^2\cos^2\bar{\phi}}. \tag{65}$$

The first term in (64) is identified as the incident beam phase at the edge. The other terms are in the form of a standard (conical) GB where the phase is sacculated along the beam axis, z_b^d, and the field exhibits a Gaussian decay off-axis along ρ_b^d, according to the complex curvature, $(z_b^d - \bar{Z}^d)^{-1}$. This condition describes a Gaussian diffraction cone that peaks over constant $\bar{\theta}$ surfaces as was shown in [31]. Numerical examples are given in Section IV.

D. Observation Points in the Transition Regions

For observation points that are near the shadow and reflection transition regions, the Heaviside functions in (28) and (29) have sharp boundaries, and the diffraction coefficients in (33) are discontinuous. Thus, we cannot evaluate the integrals in (28), (29), and (33) separately. In order to overcome this difficulty, we use the continuity of the PW solution. Over these boundaries, the sum of the diffraction and the GO PW solution is continuous (see [21]). There are four terms of diffraction, each of them is discontinuous over the shadow boundary, the reflection from the $\phi = 0$ surface, or from the $\phi = N\pi$ surface, while the other three are continuous.

First, we discuss the shadow boundary of the incident beam for the $\phi = 0$ surface. Near this boundary $\phi - \tilde{\phi}_0 \sim -\pi$, and the corresponding Heaviside functions in (28) and (29) are discontinuous. Furthermore, the term $\cot\left[(\pi + \phi - \tilde{\phi}_0)/2N\right]$ in the diffraction coefficient in (33) is singular. Note that the other two terms of the GO field in (28) and (29) and the other three diffraction coefficients in (33) are continuous. Thus, their asymptotic evaluations in (41), (48), and (52) are valid.

In order to evaluate the two discontinuous terms, we sum over the corresponding asymptotic terms in (28) and (52), similar to the procedure in [21]. Next we apply the small argument approximation of the transition function [21]

$$F(x) \approx \exp[j(\pi/4 + x)] \times \left[\sqrt{\pi x} - 2x\exp(j\pi/4) - 2x^2\exp(-j\pi/4)/3\right]. \tag{66}$$

Therefore, over the shadow and reflection boundaries, the discontinuous diffraction term in (33) can be approximated by

$$\begin{aligned}\tilde{D}_{s,h}(\phi)\sqrt{\kappa_t}/\sqrt{\rho} &= F[k_t\rho a^+(\tilde{\Phi}^-)]d^+(\tilde{\Phi}^-)/\sqrt{\rho\kappa_t} \\ &\approx \tilde{d}^{\mathrm{trn}}\exp[jk_t\rho + jk_t\rho\cos(\phi - \tilde{\phi}_0)]\end{aligned} \tag{67}$$

where

$$\begin{aligned}\tilde{d}^{\mathrm{trn}} = &-\frac{1}{2N\sqrt{\pi}}\cot\left[\frac{\pi - (\phi - \tilde{\phi}_0)}{2N}\right]\left|\cos\left(\frac{\phi - \tilde{\phi}_0}{2}\right)\right| \\ &\times\left[\sqrt{\pi} - 2\sqrt{\tilde{s}}\exp(j\pi/4) - \frac{2}{3}\tilde{s}^{1.5}\exp(-j\pi/4)\right]\end{aligned} \tag{68}$$

with

$$\tilde{s} = 2k_t\rho\cos^2[(\phi - \tilde{\phi}_0)/2]. \tag{69}$$

By using trigonometric identities and (20), the last exponent's argument in (67) can be written as $jk_t\rho + jk_t\rho\cos(\phi - \tilde{\phi}_0) = jk_t\rho - jk\hat{\boldsymbol{\kappa}}_t\cdot\mathbf{r}$. The total phase of the corresponding diffraction field integrand is obtained by adding the phase term of (34). Therefore, near the transition regions, the total phase of the diffraction field is given by

$$\kappa_x(x - \bar{x}) - \kappa_y(y - \bar{y}) + \kappa_z(z - \bar{z}) - \tilde{\Omega}_b. \tag{70}$$

This phase term is identical to the incident potential in (28) and the sum of the amplitudes of the incident potential and (28) is a continuous term over the shadow boundary.

Thus, in order to evaluate the potentials in the transition regions, we combine the integrands in (28) and (33) and denote the combined potentials by $\Psi_{A/F}^{\mathrm{trn}}(\mathbf{r})$. By using (67), $\Psi_{A,F}^{\mathrm{trn}}(\mathbf{r})$ is given by

$$\begin{aligned}\Psi_{A,F}^{\mathrm{trn}}(\mathbf{r}) = \int d^2\kappa_s\tilde{\Psi}_{A_0,F_0}\frac{k}{2\pi j\Gamma}\exp\left(-jk\tilde{\Omega}_i^{\mathrm{GO}}\right) \\ \times\left[U(\pi - |\phi - \tilde{\phi}_0|) + \tilde{d}^{\mathrm{trn}}\right]\end{aligned} \tag{71}$$

where $\tilde{\Omega}_i^{\mathrm{GO}}$ is given in (30). Comparing (71) with (28), one can see that these two integrals have an identical phase terms and differ only in their amplitudes. Thus, the asymptotic evaluation of (71) is obtained by adding to the Heaviside function in (40) the term d^{trn} that is sampled at $\bar{\theta}_0, \bar{\phi}_0$.

The total potentials over this boundary are obtained by using (71) in (26), i.e.,

$$\Psi_{A/F}(\mathbf{r}) = \Psi_{A/F}^{\mathrm{trn}}(\mathbf{r}) \mp \Psi_{A/F}^{r1} \mp \Psi_{A/F}^{r2} + \Psi_{A/F}^{d} \tag{72}$$

where $\Psi_{A/F}^d$ is obtained by replacing in (56) $\bar{D}_{s,h}$ with

$$\begin{aligned}\bar{D}_{s,h}(\phi) = (\sin\bar{\theta}_0)^{-1}\big\{&d^-(\bar{\Phi}^-)F\left[k_t\sin\bar{\theta}_0\rho a^-(\bar{\Phi}^-)\right] \\ &+ \tau d^+(\bar{\Phi}^+)F\left[k_t\sin\bar{\theta}_0\rho a^+(\bar{\Phi}^+)\right] \\ &+ \tau d^-(\bar{\Phi}^+)F\left[k_t\sin\bar{\theta}_0\rho a^-(\bar{\Phi}^+)\right]\big\}.\end{aligned} \tag{73}$$

Finally, we discuss the validity of the results above. The small argument approximation in (66) is valid for $\tilde{s} < 1$ [21]. Recalling that contributing spectral interval to the integral near the stationary point is of the order of

$$\tilde{\Delta}_{\kappa_s} \sim 2\pi/\left(k\sqrt{\det\mathbf{q}_{2\kappa_s}}\right) \sim 2\pi/\left[k^2 w_{x_b}(z_b)w_{y_b}(z_b)\right] \tag{74}$$

we conclude that the results above are valid for observation points that satisfy $\tilde{s} < 1$ for all κ_s in the spectral interval $[\bar{\kappa}_s - \tilde{\Delta}_{\kappa_s}, \bar{\kappa}_s + \tilde{\Delta}_{\kappa_s}]$. Similar analysis can be performed for the other three boundaries.

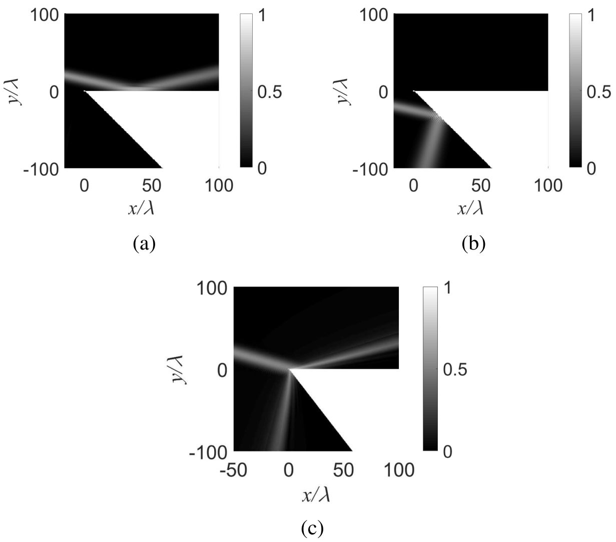

Fig. 4. Total potentials. (a) Reflection from the $\phi = 0$ surface. (b) Reflection from the $\phi = N\pi$ surface. (c) Reflection and diffraction from the tip. Note that in (a) and (b), the incident beam is impinging on the wedge far from the edge and no significant diffraction is visible.

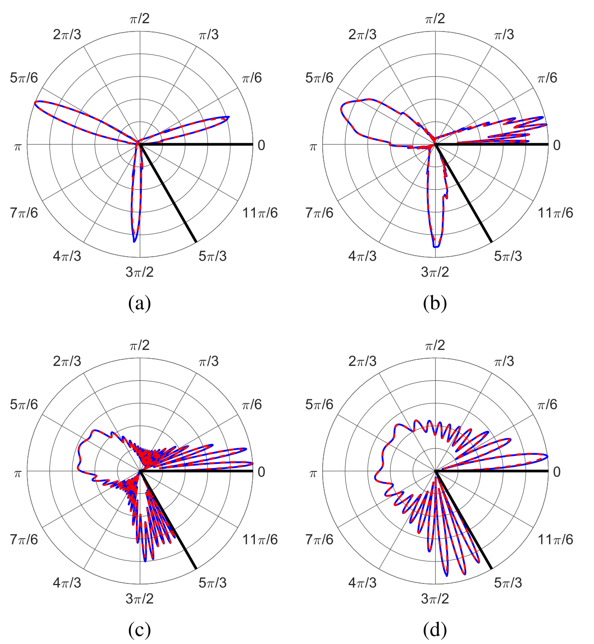

Fig. 5. Comparison of the amplitudes of total asymptotic potential (solid lines) to the reference solution in (28), (29), and (33) (dashed lines) for the beam parameters in Fig. 4(c) over radii (a) $r = 50\lambda$, (b) $r = 20\lambda$, (c) $r = 10\lambda$, and (d) $r = 5\lambda$.

IV. Numerical Examples

In order to illustrate the asymptotic results, we plot the absolute value of the electric potential $|\Psi_A|/\max(|\Psi_A|)$ for several sets of parameters. Reflections from the wedge surfaces are plotted in Fig. 4(a) and (b). Here, we have used $\Gamma = -j\pi/10\lambda$, $\alpha = \pi/3$, $\bar{\phi} = 1.88\pi$, and $\bar{\theta} = \pi/2$ so that the beam is propagating in the direction of $\hat{\bar{\kappa}} = (\cos\bar{\phi}, \sin\bar{\phi}, 0)$. In Fig. 4(a), the beam is emanating from $\bar{y} = 20\lambda$, $\bar{x} = -15\lambda$ and in Fig. 4(b), we have set $\bar{y} = -20\lambda$, $\bar{x} = -15\lambda$. Note that no significant diffraction is present in the electric potentials in either Fig. 4(a) or (b).

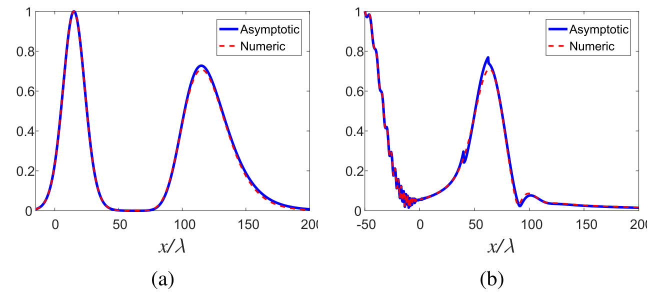

Fig. 6. Comparison of the amplitudes of the total asymptotic potential to the reference one for observation points over $y = 20\lambda$ for the beam parameters in (a) Fig. 4(a) and (b) Fig. 4(c).

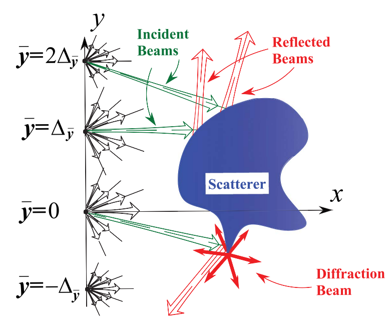

Fig. 7. Phase space beam summation for scattering from complex objects. The incident beam is decomposed into a discrete set of GBPs that interacts locally with the scatterer. The scattered field is obtained by summing over all scattered GBPs. In the figure, the lower GBP–scatterer interaction is of a wedge type that includes a scattered GB and a diffraction beam.

Next in Fig. 4(c) we illustrate the diffraction phenomenon. To that end we set $\Gamma = -j/30\lambda$, $\alpha = \pi/3$, $\bar{\phi} = 1.88\pi$, $\bar{y} = 20\lambda$, and $\bar{x} = -50.35\lambda$. This set of parameters yields $\eta = 0$ so that the resulting incident beam axis intersects the wedge at the edge.

In order to validate the asymptotic analysis in Section III, we compare the asymptotic potentials with a reference solution that is calculated by numerically integrating over the spectral integrals in (28), (29), and (33). The sum of these integrals is compared with the total asymptotic potential using the beam parameters in Fig. 4(c). For clarity, fields are normalized by the maximum of the reference solution.

The results for observation points over the circles $r = 50\lambda$, 20λ, 10λ, and 5λ are presented in Fig. 5(a)–(d), respectively. Clearly the asymptotic solution (solid lines) and the reference one (dashed lines) reveal good agreement both near and far from the wedge top, verifying all asymptotic potentials types.

The asymptotic potentials presented here are not uniform solutions as stated in Sections III-C and III-D. To demonstrate the transition between the solutions, we compare in Fig. 6(a) and (b) the asymptotic solution with the reference one for observation points over the line $y = 20\lambda$, for the beam parameters in Fig. 4(a) and (c), respectively. The asymptotic solutions are discontinuous. This is clearly apparent in Fig. 6(b) since these set of parameters yield a beam that hits the wedge at the top. The transition region was chosen to be $\bar{s} < 1$ where $\bar{s}$ is obtained by sampling $\tilde{s}$ in (69) on-axis.

V. Conclusion

The GB summation method is widely recognized nowadays as an important tool for the analysis and synthesis of EM wave propagation and scattering. Under this framework, the incident field is decomposed into a discrete set of GBPs. The main advantage of this method arises from the local GBPs–scatterer interactions that can yield closed form (asymptotic) solutions. Thus, the scatterer can be considered as composed from different basic shapes, and the scattered field can be evaluated by resolving each GBP interaction with one of these shapes as described in Fig. 7. To that extent, a set of solutions to canonical problems, such as the one presented in this paper, is required.

References

[1] A. Shlivinski, E. Heyman, A. Boag, and C. Letrou, "A phase-space beam summation formulation for ultrawide-band radiation," *IEEE Trans. Antennas Propag.*, vol. 52, no. 8, pp. 2042–2056, Aug. 2004.

[2] T. Melamed, "Exact beam decomposition of time-harmonic electromagnetic waves," *J. Electromag. Waves Appl.*, vol. 23, pp. 975–986, 2009.

[3] T. Melamed, "TE and TM beam decomposition of time-harmonic electromagnetic waves," *J. Opt. Soc. Amer. A, Opt. Image Sci.*, vol. 28, no. 3, pp. 401–409, 2011.

[4] J. J. Maciel and L. B. Felsen, "Gaussian beam analysis of propagation from an extended plane aperture distribution through dielectric layers. I. Plane layer," *IEEE Trans. Antennas Propag.*, vol. 38, no. 10, pp. 1607–1617, Oct. 1990.

[5] J. A. Lock, "Scattering of a diagonally incident focused Gaussian beam by an infinitely long homogeneous circular cylinder," *J. Opt. Soc. Amer. A*, vol. 14, no. 3, pp. 640–652, 1997.

[6] H. T. Anastassiu and P. H. Pathak, "Closed form solution for three-dimensional reflection of an arbitrary Gaussian beam by a smooth surface," *Radio Sci.*, vol. 37, pp. 1–8, Apr. 2002.

[7] I. Tinkelman and T. Melamed, "Gaussian-beam propagation in generic anisotropic wave-number profiles," *Opt. Lett.*, vol. 28, no. 13, pp. 1081–1083, 2003.

[8] I. Tinkelman and T. Melamed, "Local spectrum analysis of field propagation in an anisotropic medium. Part I. Time-harmonic fields," *J. Opt. Soc. Amer. A*, vol. 22, no. 6, pp. 1200–1207, 2005.

[9] I. Tinkelman and T. Melamed, "Local spectrum analysis of field propagation in an anisotropic medium. Part II. Time-dependent fields," *J. Opt. Soc. Amer. A*, vol. 22, no. 6, pp. 1208–1215, 2005.

[10] H. Zhang and Y. Han, "Scattering by a confocal multilayered spheroidal particle illuminated by an axial Gaussian beam," *IEEE Trans. Antennas Propag.*, vol. 53, no. 4, pp. 1514–1518, Apr. 2005.

[11] Y. Hadad and T. Melamed, "Non-orthogonal domain parabolic equation and its tilted Gaussian beam solutions," *IEEE Trans. Antennas Propag.*, vol. 58, no. 4, pp. 1164–1172, Apr. 2010.

[12] Y. Hadad and T. Melamed, "Parameterization of the tilted Gaussian beam waveobjects," *Prog. Electromagn. Res.*, vol. 102, pp. 65–80, 2010.

[13] Y. Hadad and T. Melamed, "Tilted Gaussian beam propagation in inhomogeneous media," *J. Opt. Soc. Amer. A*, vol. 27, no. 8, pp. 1840–1850, 2010.

[14] Z.-S. Wu, Z.-J. Li, H. Li, Q.-K. Yuan, and H.-Y. Li, "Off-axis Gaussian beam scattering by an anisotropic coated sphere," *IEEE Trans. Antennas Propag.*, vol. 59, no. 12, pp. 4740–4748, Dec. 2011.

[15] E. Mizrahi and T. Melamed, "Plane wave spectral analysis of scattering of an EM Gaussian beam by a moving PEC circular cylinder," in *Proc. IEEE 27th Conv. Elect. Electron. Eng. Isr.*, Nov. 2012, pp. 1–4.

[16] R. Tuvi and T. Melamed, "Gaussian beam diffraction by a fast moving wedge," in *Proc. Int. Symp. Electromagn. Theory*, May 2013, pp. 901–904.

[17] R. Tuvi, E. Heyman, and T. Melamed, "Beam frame representation for ultrawideband radiation from volume source distributions: Frequency-domain and time-domain formulations," *IEEE Trans. Antennas Propag.*, vol. 67, no. 2, pp. 1010–1024, Feb. 2019.

[18] A. Sommerfeld, "Asymptotische Darstellung von Formeln aus der Beugungstheorie des Lichtes," *J. Für Die Reine Und Angew. Mathematik*, vol. 158, pp. 199–208, Jun. 1927.

[19] J. B. Keller, "Geometrical theory of diffraction," *J. Opt. Soc. Amer.*, vol. 52, no. 2, pp. 116–130, 1962.

[20] P. H. Pathak and R. G. Kouyoumjian, "The dyadic diffraction coefficient for a perfectly conducting wedge," Columbus Electrosci. Lab, Ohio State Univ., Columbus, OH, USA, Tech. Rep. TR-2183-4, 1970, pp. 1–87.

[21] R. G. Kouyoumjian and P. H. Pathak, "A uniform geometrical theory of diffraction for an edge in a perfectly conducting surface," *Proc. IEEE*, vol. 62, no. 11, pp. 1448–1461, Nov. 1974.

[22] F. Hacivelioglu, L. Sevgi, and P. Y. Uiimtsev, "Electromagnetic wave scattering from a wedge with perfectly reflecting boundaries: Analysis of asymptotic techniques," *IEEE Antennas Propag. Mag.*, vol. 53, no. 3, pp. 232–253, Jun. 2011.

[23] M. Katsav and E. Heyman, "Phase space Gaussian beam summation analysis of half plane diffraction," *IEEE Trans. Antennas Propag.*, vol. 55, no. 6, pp. 1535–1545, Jun. 2007.

[24] M. Katsav and E. Heyman, "Gaussian beam summation representation of a two-dimensional Gaussian beam diffraction by a half plane," *IEEE Trans. Antennas Propag.*, vol. 55, no. 8, pp. 2247–2257, Aug. 2007.

[25] M. Katsav and E. Heyman, "Gaussian beams summation representation of half plane diffraction: A full 3-D formulation," *IEEE Trans. Antennas Propag.*, vol. 57, no. 4, pp. 1081–1094, Apr. 2009.

[26] M. Katsav and E. Heyman, "Gaussian beam summation representation of beam diffraction by an impedance wedge: A 3D electromagnetic formulation within the physical optics approximation," *IEEE Trans. Antennas Propag.*, vol. 60, no. 12, pp. 5843–5858, Dec. 2012.

[27] M. Katsav, E. Heyman, and L. Klinkenbusch, "Beam diffraction by a wedge: Exact and complex ray solutions," *IEEE Trans. Antennas Propag.*, vol. 62, no. 7, pp. 3731–3740, Jul. 2014.

[28] M. Katsav and E. Heyman, "Converging and diverging beam diffraction by a wedge: A complex-source formulation and alternative solutions," *IEEE Trans. Antennas Propag.*, vol. 64, no. 7, pp. 3080–3093, Jul. 2016.

[29] R. Tuvi and T. Melamed, "Asymptotic analysis of plane wave scattering by a fast moving PEC wedge," *IEEE Trans. Antennas Propag.*, vol. 65, no. 7, pp. 3638–3644, Jul. 2017.

[30] T. Melamed, "Phase-space beam summation: A local spectrum analysis of time-dependent radiation," *J. Electromagn. Waves Appl.*, vol. 11, no. 6, pp. 739–773, 1997.

[31] E. Heyman and R. Ianconescu, "Pulsed beam diffraction by a perfectly conducting wedge: Local scattering models," *IEEE Trans. Antennas Propag.*, vol. 43, no. 5, pp. 519–528, May 1995.

Ram Tuvi was born in Holon, Israel, in 1982. He received the B.Sc. and M.Sc. *(cum laude)* degrees in electrical and computer engineering from the Ben-Gurion University of the Negev, Beer Sheva, Israel, in 2010 and 2013, respectively, and the Ph.D. degree from the School of Electrical Engineering, Tel-Aviv University, Tel Aviv, Israel, in 2019.

He currently holds a post-doctoral position with the Jackson School of Geosciences, University of Texas at Austin, Austin, TX, USA. His current research interests include wave theory, scattering theory, and inverse scattering.

Timor Melamed (SM'94) was born in Tel-Aviv, Israel, in 1964. He received the B.Sc. degree *(magna cum laude)* in electrical engineering and the Ph.D. degree from Tel-Aviv University, Tel-Aviv, in 1989 and 1997, respectively.

From 1996 to 1998, he held a post-doctoral position with the Department of Aerospace and Mechanical Engineering, Boston University, Boston, MA, USA. He is currently with the School of Electrical and Computer Engineering, Ben-Gurion University of the Negev, Beer Sheva, Israel. His current research interests include analytic techniques in wave theory, transient wave phenomena, inverse scattering, and electrodynamics.